J. Fluid Mech. (1992), *vol.* 239, *pp.* 1–21
Printed in Great Britain

The electrohydrodynamic deformation of drops suspended in liquids in steady and oscillatory electric fields

By O. VIZIKA AND D. A. SAVILLE
Department of Chemical Engineering, Princeton University, Princeton, NJ 08544, USA

(Received 13 May 1991 and in revised form 19 November 1991)

When an electric field is applied to a drop suspended in another liquid the drop deforms. The relation between the applied field and the mode and magnitude of the deformation have been studied extensively. Nevertheless, Torza, Cox & Mason (1971) found that quantitative agreement between the leaky dielectric theory (Taylor 1966) and experiment is quite poor. Here we describe results from a new series of experiments. Drops suspended in weakly conducting liquids were deformed into spheroids with both steady and oscillatory fields. Drop deformation, interfacial tension, and the electrical properties of the fluids were measured for each system to provide a definitive test of the theory. The agreement between the leaky dielectric model and our results for drop deformations in steady fields is much improved over previous results, although discrepancies remain for some systems. Drop deformations in oscillatory fields consist of steady and oscillatory parts because of the quadratic dependence on the field strength. Measurements of the steady part at 60 Hz, where the oscillatory deformation is negligible, are in excellent agreement with the theory. The effects of frequency on the steady deformation were studied by measuring oblate deformations at a series of frequencies and field strengths; the agreement with theory is good. Finally, the time-dependent total deformation was measured under conditions where both parts of the deformation are commensurate. Good agreement was found between the measured and predicted maximum and minimum deformations. Nevertheless, only a small range of fluid properties could be studied owing to the need to avoid droplet sedimentation.

1. Introduction

Electrohydrodynamics is the study of fluid motions driven by external electrostatic fields. The deformation of fluid interfaces, especially the behaviour of drops in external fields, has been studied extensively. Part of the early interest derived from applications, including the deformation and breakup of raindrops in thunderstorms and the breakdown of dielectric liquids due to contaminants such as water droplets. Melcher & Taylor (1969) summarize early developments in the area while surveys by Melcher (1976) and Arp, Foister & Mason (1980) provide somewhat more recent perspectives. Melcher's *Continuum Electromechanics* (1981) contains a lucid development of theoretical aspects. Contemporary work ranges from experiments on the modification of polymer blends (Moriya, Adachi & Kotaka 1985 and Venugopal, Krause & Wnek 1989), drop deformation (Moriya, Adachi & Kotaka 1986 and Nishiwaki, Adachi & Kotaka 1988), fibre spinning (Larrendo & St John Manley 1981) and the enhancement of solvent extraction processes (Scott & Wham 1989) to

theoretical studies of free-surface-driven flows (Basaran & Scriven 1988), drop deformation and breakup (Sherwood 1988), and compound droplets (Oguz & Sadhal 1989). Despite this interest, the experimental foundation of the subject is weak. Relatively few experiments have been reported and none display much quantitative agreement with the extant theory. Here we concentrate on the deformation of drops suspended in poorly conducting liquids.

When an uncharged drop is suspended in a dielectric liquid in an external electric field there is discontinuity in the field at the drop interface. In the classical electrostatic model, where the fluids are treated as perfectly insulating dielectrics, the electric stress is always normal to the interface. This stress can be balanced by the interfacial tension, so the fluids remain motionless and the deformation is prolate (O'Konski & Thacher 1953; Garton & Krasucki 1964). However, experiments by Allan & Mason (1962) produced both prolate and oblate droplets. More specifically, Allan & Mason observed that conducting drops deformed into prolate spheroids, in agreement with predictions based on the electrostatic theory, but some dielectric drops deformed into oblate spheroids. A new line of reasoning was introduced by Taylor (1966), who proposed what came to be known as the leaky dielectric theory or model. In this model the liquids have small conductivities so, when an electric field is applied, free charge appears at the drop interface. However, the charge on the two hemispheres of a drop in a uniform field is antisymmetric so the net charge is zero. The action of the electric field on this charge sets the fluids in motion and toroidal circulation patterns are formed inside and outside the droplet. Taylor's model was able to predict both prolate and oblate deformations – depending on the properties of the fluids – in qualitative agreement with the previous experiments.

Later, extensive experimental work by Torza, Cox & Mason (1971) revealed deformations much larger than those predicted theoretically, in most cases by a factor of two to four. Since the theory is linearized to address small deformations, nonlinear effects could be a factor. However, extending the theory to include higher-order terms failed to resolve the disagreement (Ajayi 1978) and the lack of general agreement between theory and experiment persists to this day.

Another explanation was offered by Torza *et al.* (1971), who suggested that electrokinetic phenomena could be responsible for the discrepancies. Ion transport produces a charged interface so counterions in the adjacent fluid form a diffuse charge layer in each phase. Their structure is determined by a balance between the thermal motion of the ions and electrostatic forces. Additional flows and stresses then arise from the action of the applied field on the charge cloud. Baygents & Saville (1989) developed an electrokinetic theory which deals with the issues raised by Torza *et al.* However, even though the stresses and microscale motions are more complicated than in the leaky dielectric theory, it turns out that the deformation calculated for a drop with no net charge is exactly the same as that calculated using the leaky dielectric model. Accordingly, when there is no net charge on the drop, the leaky dielectric theory is the correct lumped-parameter model and since none of the obvious theoretical extensions resolve matters, it seems prudent to carry out further experiments to test the theory. Here we present the results of an experimental study of drop deformation in steady and oscillatory electric fields.

The theoretical background is reviewed in §2, which includes the requisite formulae for steady and oscillatory fields. In §3, we discuss experimental procedures and drop deformations studied over a range of fluid conductivities in steady fields. In oscillatory fields, the effects of field intensity and frequency on time-dependent and time-independent parts of the deformation were studied for a smaller set of fluid

pairs. The results are discussed and reasons for the remaining discrepancies advanced in §§4 and 5.

2. Theoretical background

2.1. *The leaky dielectric model*

To explain the behaviour of a spheroidal drop suspended in another liquid, Taylor (1966) suggested that the fluids be treated as dielectrics with an Ohmic resistance; conduction processes produce free charge on the interface(figure 1) and the action of the field on the charge sets the fluids into motion. The main points of the leaky dielectric theory are outlined here using an adaptation of Taylor's (1966) notation, which differs from that of Torza *et al.* (1971).

Consider two isopycnic, immiscible fluids. A drop of fluid with undeformed radius a is suspended in another fluid (overbars will be used to identify the drop phase). Viscosities are denoted by μ, dielectric constants by ϵ, and conductivities by σ. The liquid–liquid interface is characterized by a uniform interfacial tension, γ. The shape of the drop is calculated by determining the deformation necessary to balance the stresses due to the electric field and flow.

The fluids have uniform properties and there is no free charge in the bulk phases so the electric field is described by solutions to Laplace's equation inside and outside the drop. The conditions placed on the potential are: (*a*) the field is finite, (*b*) the tangential electric field is continuous at the interface, (*c*) the conduction current normal to the interface is continuous, and (*d*) far from the drop the field has a uniform magnitude, E_0. The components of the net electric stress at the drop interface (i.e. the jumps in the electric stress across the interface) are

$$\left.\begin{aligned}[T_r^{\mathrm{e}}] &= \frac{9E_0^2\epsilon_0}{2(2+R)^2}[\bar{\epsilon}-\epsilon+\{\epsilon(R^2+1)-2\bar{\epsilon}\}\cos^2\theta],\\ [T_\theta^{\mathrm{e}}] &= -\frac{9E_0^2\epsilon_0}{(2+R)^2}(\epsilon R-\bar{\epsilon})\cos\theta\sin\theta\end{aligned}\right\} \tag{1}$$

in spherical coordinates with θ denoting the angle measured from the rear of the drop (Taylor 1966); ϵ_0 is the permittivity of free space and $R \equiv \bar{\sigma}/\sigma$ is the ratio of conductivities.

The charge arising on the interface to compensate for the jump in the normal component of the electric field is

$$\rho^{(\mathrm{e})} = 3\epsilon_0 E_0 \cos\theta\left(\frac{\epsilon R-\bar{\epsilon}}{2+R}\right). \tag{2}$$

Equation (2) shows that the total charge on the drop is zero but the drop hemispheres facing the electrodes become positively or negatively charged depending on the sign of $(\epsilon R-\bar{\epsilon})$.

If the velocity is small, the Stokes equations describe flow inside and outside the drop. The boundary conditions imposed at the drop interface are the continuity of velocity and stress. The jumps in the radial and tangential viscous stress at the drop interface are

$$\left.\begin{aligned}[T_r^{\mathrm{v}}] &= \frac{9E_0^2\epsilon_0\bar{\epsilon}(SR-1)}{10(2+R)^2(\mu+\bar{\mu})}(2\mu+3\bar{\mu})(1-3\cos^2\theta),\\ [T_\theta^{\mathrm{v}}] &= \frac{9E_0^2\epsilon_0\bar{\epsilon}}{(2+R)^2}(SR-1)\cos\theta\sin\theta,\end{aligned}\right\} \tag{3}$$

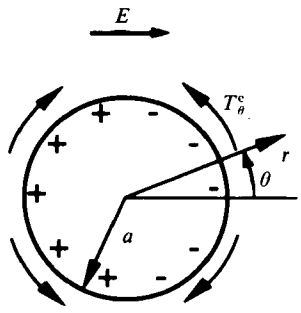

FIGURE 1. Schematic representation of a liquid drop suspended in an infinite liquid dielectric deformed under the action of an electric field. Here $(\epsilon R - \bar{\epsilon})$ is negative.

where $S = \epsilon/\bar{\epsilon}$. Further details are given by Taylor (1966) and by Melcher & Taylor (1969).

For a slightly deformed interface the radial stress balance can be used to calculate the deformation. Let the drop deformation, D, be defined by

$$D = \frac{d_1 - d_2}{d_1 + d_2}, \tag{4}$$

where d_1 and d_2 are the lengths of drop axes parallel and perpendicular to the applied field. For small deformations the drop takes the shape of a spheroid, namely

$$r = a\{1 + \tfrac{2}{3}D(3\cos^2\theta - 1)\}, \tag{5}$$

where a is the radius of the undeformed drop. The balance of radial stresses on the drop interface requires that

$$[T^e_r] + [T^v_r] - \gamma C = 0, \tag{6}$$

where γC is the radial force density due to interfacial tension with C denoting the curvature of the interface, and the deformation is given by

$$\left.\begin{aligned} D = maE_0^2, \qquad m \equiv \frac{9\epsilon_0 \bar{\epsilon}}{16\gamma} \frac{\Phi}{(2+R)^2}, \\ \Phi \equiv S(R^2+1) - 2 + 3(SR-1)\frac{2M+3}{5M+5}. \end{aligned}\right\} \tag{7}$$

Φ is Taylor's 'discriminating function' and $M \equiv \mu/\bar{\mu}$. If the fluid parameters are adjusted such that $\Phi = 0$ the drop retains its spherical shape. $\Phi > 0$ means $d_1 > d_2$ and the drop takes on a prolate form; for $\Phi < 0$, $d_1 < d_2$ and the drop is deformed into an oblate spheroid.

A schematic representation of a drop under a uniform external electric field is shown in figure 1, which depicts the charge distribution for the case where $(\epsilon R - \bar{\epsilon})$ is negative, e.g. the outer fluid is more conductive than the inner fluid. Here the hemisphere facing the negative electrode is negatively charged, the tangential electric stress is positive, and flow is from the poles to the equator.

2.2. *The leaky dielectric model for oscillatory fields*

Torza *et al.* (1971) extended Taylor's model to include situations where the applied field varies with time as

$$E = E_0 \cos \omega t \tag{8}$$

and $\omega = 2\pi f$ is the angular frequency of the field. As can be seen from (1), even though the electric field at the drop interface is time-dependent, the electric stress has both steady and time-dependent components. Thus, the total drop deformation, D, has steady and time-dependent components, D_s and D_t. By considering both the steady and the time-dependent parts of the normal stress on the interface, Torza *et al.* calculated the total deformation, namely

$$D = D_s + D_t. \tag{9}$$

For the steady component of the stress, the deformation is given by equations similar to (7), namely

$$D_s = \frac{9\epsilon_0 \epsilon}{16\gamma} \Phi_s a \bar{E}_0^2 \tag{10}$$

except that

$$\Phi_s \equiv 1 - \frac{S^2R(11+14M)+15S^2(1+M)+S(19+16M)+15R^2S\tau^2\omega^2(M+1)(S+2)}{5(M+1)[S^2(2+R)^2+R^2\tau^2\omega^2(1+2S)^2]} \tag{11}$$

and $\bar{E}$ is the root-mean-square field strength. Here $\tau \equiv \epsilon_0 \epsilon/\bar{\sigma}$ denotes a relaxation time; for $\omega = 0$ these formulae reduce to (7) since $\bar{E} = E_0$. For the time-dependent part,

$$\left.\begin{aligned}
&D_t \equiv D_s\left\{\frac{I\cos(2\omega t+\beta)}{\Phi_s(1+k^2\lambda_2^2)^{\frac{1}{2}}}\right\},\\
&I \equiv \left\{\Phi_s^2+\frac{R^2S\tau^2\omega^2(SR-1)^2(19+16M)[20(M+1)-S(4M+1)]}{25(M+1)^2[S^2(2+R)^2+R^2\tau^2\omega^2(1+2S)^2]^2}\right\}^{\frac{1}{2}}\\
&k \equiv \omega\mu a/\gamma\\
&\cos\beta \equiv \frac{h^*+\overline{(h^*)}}{2I}, \quad \sin\beta \equiv \frac{h^*-\overline{(h^*)}}{2\,\mathrm{i}I}, \quad h^* \equiv \frac{F_r^*-\lambda_1 F_\theta^*}{1+\mathrm{i}k\lambda_2},\\
&F_r^* \equiv \frac{A^2(5S-2)}{S}-2A+1, \quad F_\theta^* \equiv \frac{RS^2(1+\mathrm{i}\tau\omega R)}{[(2+R)S+\mathrm{i}\tau\omega(1+2S)R]^2},\\
&\lambda_1 \equiv \left(\frac{1}{SR}-1\right)\frac{3(2M+3)}{5(M+1)}, \quad \lambda_2 \equiv \frac{(16M+19)(3M+2)}{20(M+1)},\\
&A \equiv \frac{S(1+\mathrm{i}\tau\omega R)}{(2+R)S+\mathrm{i}\tau\omega(1+2S)R}.
\end{aligned}\right\} \tag{12}$$

The overbars denote complex conjugates. These formulae were used in the comparisons between theoretical and experimental results.

3. Experimental programme

3.1. *Materials and experimental procedures*

3.1.1. *Apparatus*

The experiments described here were carried out as part of an ongoing study of electrohydrodynamics; our system works as follows. Drops are suspended in a rectangular glass cell equipped with two flat brass electrodes (4 × 4 cm, about 0.1 cm in thickness) mounted opposite each other. The separation distance is adjustable and

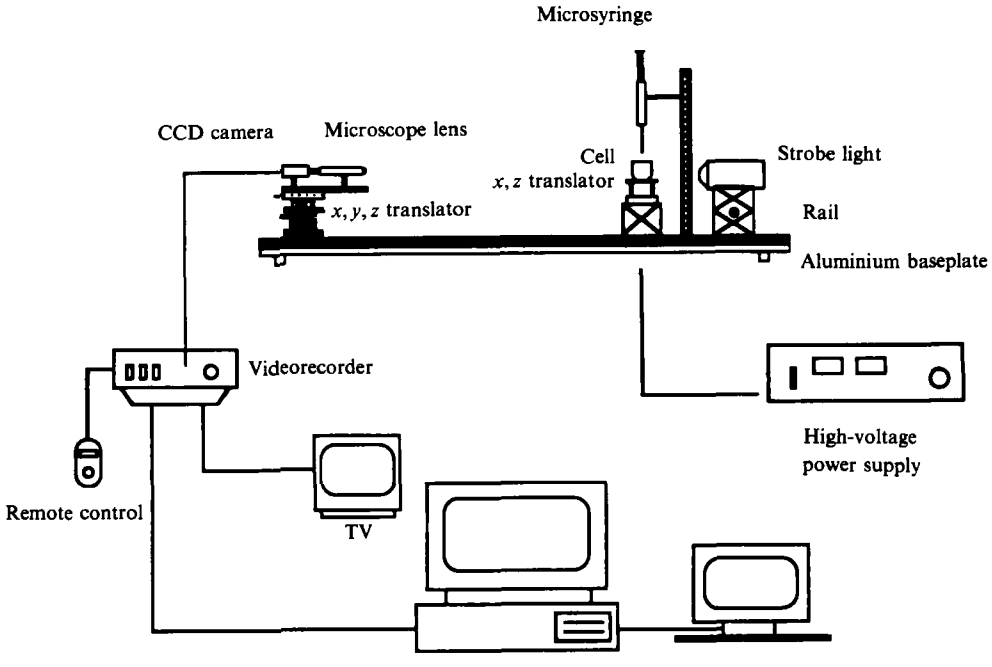

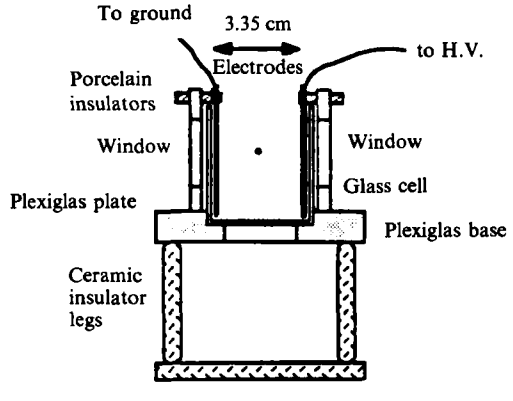

FIGURE 2. Schematic diagram of the experimental set-up.

is usually 3.35 cm. A schematic diagram of the experimental set-up is shown in figure 2. Small drops (the drop diameter seldom exceeds 1 mm) experience a uniform field if suspended in the central region of the cell. An electric field is applied across the electrodes from a Spellman power supply; field strengths range from 0 to 4.5 kV/cm. Where an oscillating field is needed, a Trek oscillating voltage supply/amplifier is used (output voltage ± 20 kV).

The cell is mounted on a (x, z)-translator-rotator system and the digital camera (Ikegami CCD) and the microscope lens are mounted on an (x, y, z)-translator system. Both systems are mounted on a rail for stability. This set-up allows rough

alignment and adjustment of the distance between the cell and the optical observation system. The fine alignment and focusing are made with micrometer screws on the translators.

An electrometer connected in series to the network (after the low-voltage electrode) enables us to measure the current continuously. In this way, the resistance of the cell can be calculated and changes due to aging, impurities, or the effect of the electric field monitored.

The voltage applied to the high-voltage electrode can be measured directly with an oscilloscope using a high-voltage probe connected to the electrode, or calculated from the Spellman reading minus the voltage drop in the leads. Either method gives the same result.

3.1.2. *Experimental procedure*

The fluids are chosen so that the host fluid has either the same density as the suspended drop or a very high viscosity so that drops rise or fall very slowly. Drops are released in the host fluid from a microsyringe held by a clamp mounted on a rod. After a drop is released, the microsyringe is removed and an image of the quiescent drop captured. Then the power supply is turned on and the output voltage increased systematically. For each value of the applied field, an image of the deformed drop is captured after the drop has reached steady state (this is extremely important when the host fluid is very viscous, and the drop may need several seconds to obtain the final shape). The drop images from the CCD camera are sent to the Matrox frame grabber board which converts the video image to a 640 by 480 pixel digital image; single drops usually occupy an area 200–300 pixels on a side, although larger images are used when the deformation is small. The digitized image signal is viewed with a Mitsubishi colour monitor. Drop deformations are measured using image analysis and enhancement techniques with the microsyringe tip used as a calibration object.

3.1.3. *Measurements of the physical properties of the fluids*

To attempt a rigorous comparison between theory and experiment, the properties of the fluids must be measured as accurately as possible. As can be seen from the equations given in the theoretical section, the properties to be measured are the viscosities, dielectric constants and conductivities of the liquids and the interfacial tension.

(*a*) *Dielectric constant measurements* The dielectric constant of a liquid is calculated as the ratio of the capacitance of the test cell filled with the liquid, C_s, divided by the capacitance of the same cell when empty and dry, C_v. For very accurate measurements three-terminal cells are usually used (ASTM 1987). Our measurements require easy dismantling and cleaning (many of the liquids are very viscous oils), so the three-terminal idea was abandoned and a simple two-terminal cell designed. The cell consists of two Teflon plates separated by a 5 cm diameter Plexiglas tube. The aluminium electrodes are 4.5 cm in diameter and separated by a 0.3 cm, gap. With this cell the measured capacitance includes contributions from the Teflon plates and liquid outside the electrodes. It turns out that this capacitance can be as much as 20% of the total capacitance of the empty cell. Obviously the accuracy of these measurements cannot be the same as that of the measurements with three-terminal cells. However, calibration of this cell with a liquid of high purity and known dielectric constant can assure enough accuracy for our purposes; the accuracy is better than 1%, with a reproducibility of 0.1%. The procedure is to use a constant volume of liquid and to assume that the capacitance extraneous to this

Fluid system: drop/host	Dielectric constant ratio $S = \epsilon/\bar{\epsilon}$	Conductivity ratio $R = \bar{\sigma}/\sigma$	Viscosity ratio† $M = \mu/\bar{\mu}$	Interfacial tension γ (dyne/cm)
Water/Castor oil	4.45/78.3 = 0.057	$>10^4$	14/0.01 = 1400	16.8
Water/Silicone oil (300 P)	2.75/78.3 = 0.035	$>10^4$	$300/0.01 = 3\times10^4$	28.3
Water/Silicone (1000 P)	2.75/78.3 = 0.035	$>10^4$	$1000/0.01 = 10^5$	28.3
Water+Triton/Castor oil (non-equilibrated)	4.45/78.3 = 0.057	$>10^4$	14/0.35 = 40	1.5
Water+Triton Castor oil (equilibrated)	4.58/78.3 = 0.059	$>10^4$	14/0.35 = 40	1.59
Water+Triton/Silicone oil (125 P) (equilibrated)	2.76/78.3 = 0.035	$>10^4$	125/0.35 = 357	4.25
Castor oil/Silicone oil (100 P)	2.75/4.45 = 0.62	>30	100/14 = 7.14	4.61
Silicone oil (50 P)/Castor oil+Triton	5.6/2.75 = 2.04	$<10^{-4}$	10/50 = 0.2	4.25
Silicone oil (125 P)/Castor oil+Triton	5.6/2.75 = 2.04	$<10^{-4}$	10/125 = 0.08	4.25
Silicone oil (10 P)/Castor oil	4.45/2.75 = 1.62	$<10^{-2}$	14/10 = 1.4	4.61
Silicone oil (125 P)/Castor oil	4.45/2.75 = 1.62	$<10^{-2}$	14/124 = 0.112	4.61

† Viscosities of the castor oil- and water-surfactant mixtures were measured with a capillary viscometer.

TABLE 1. Physicochemical and electric properties

volume is constant. If C_e denotes the capacitance extraneous to the fixed volume, then the dielectric constant of the fluid is $(C_s - C_e)/(C_v - C_e)$. From the measurement on the standard fluid, the 'extra' capacitance, C_e, is determined for the particular volume of liquid. For cell calibration, pure cyclohexane with a dielectric constant of 2.023 is used, as suggested by Hartshorn, Parry & Essen (1955). After the cell was calibrated, measurements of the dielectric constant of other pure liquids were made; they agreed with tabulated data (Margott & Smith 1951; *American Institute of Physics Handbook* 1972).

(*b*) *Interfacial tension measurements* There are several static and dynamic methods for measuring the interfacial tension between two liquids (Davis & Rideal 1963; Adamson 1967). However, for our systems, where $(\rho - \bar{\rho}) \sim 10^{-2}$ gm/cm^3, most of these methods cannot be applied. The main problem is to ensure that a large solid surface (e.g. a plate or ring) is uniformly wet by the one of the fluids. We avoid this problem by using a method where a straight platinum wire is pulled (vertically) through the liquid–liquid interface (Miller, Penn & Hedvat 1983). The force is measured using an electrobalance and easily related to the interfacial tension and perimeter of the wire, which is measured in a microscope and verified by measuring the surface tension of a standard liquid. Hexadecane was used in the results reported here since high-purity samples were available and it does not easily pick up substances that could affect the surface tension. The overall accuracy of the method was checked by measuring the interfacial tension of the water–hexadecane system.

(*c*) *Conductivity measurements* The conductivity of the fluid and its dependence on the electric field strength can be important. Ordinary conductivity meters are not appropriate since the fluid conductivities are low, 10^{-9}–10^{-13} S/m. An experimental set-up similar to that shown in figure 2 is used for our measurements. High voltage is applied when the cell is filled with the low-conductivity fluid and the current through the circuit measured by means of a sensitive ammeter (measuring down to 10^{-12} A). From the voltage–current curves, the resistance of the cell is deduced and the conductivity of the liquid calculated.

3.1.4. *Summary of the physical property measurements*

The physicochemical and electric properties of the fluid systems used in the experiments are given in table 1; all measurements werc made at room temperature. Figure 3 shows a water drop suspended in castor oil; it deforms into a prolate spheroid as the field increases from 0 to 3.5 kV/cm. An oblate silicone oil crop suspended in a mixture of castor oil and a surfactant (Triton, octylphenoxyethoxyethanol, Rohm & Haas Co.) is shown in figure 4. Large amounts of surfactant were used in some experiments to control the conductivity and lower the interfacial tension so as to provide larger deformations. In the water systems the Triton concentration was 10–12 wt.% while in the castor oil system the concentration was 35%, by volume.

3.2. *Drop deformation measurements in steady fields*

The fluid systems can be divided into three classes:

Class (i): $R \gg 1$. Fluids in this class give prolate deformations described by the simplified equation

$$D = \frac{9\epsilon_0 \epsilon}{16\gamma} a E_0^2. \tag{13}$$

This class includes systems in which the drop fluid is much more conductive than the host fluid, e.g. water drops in castor oil.

$E_0 = 0$ kV/cm, $D = 0$ $E_0 = 0.87$ kV/cm, $D = 0.0045$ $E_0 = 1.47$ kV/cm, $D = 0.0112$

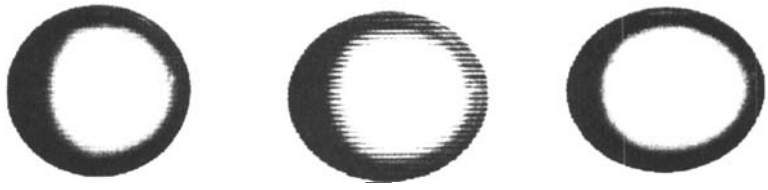

$E_0 = 2.35$ kV/cm, $D = 0.0312$ $E_0 = 2.94$ kV/cm, $D = 0.049$ $E_0 = 3.82$ kV/cm, $D = 0.087$

FIGURE 3. Sequence of pictures of a water drop suspended in castor oil; as the field increases the drop deforms into a prolate spheroid. The deformation, D, and field strength, E_0 (kV/cm), are noted on the figure; the electric field is horizontal.

$E_0 = 0.75$ kV/cm, $D = -0.002$ $E_0 = 1.25$ kV/cm, $D = -0.0083$ $E_0 = 1.97$ kV/cm, $D = -0.0166$

$E_0 = 2.45$ kV/cm, $D = -0.025$ $E_0 = 3.16$ kV/cm, $D = -0.046$

FIGURE 4. Sequence of pictures of a silicon oil drop suspended in castor oil + Triton; as the field increases the drop deforms into an oblate spheroid. The deformation, D, and field strength, E_0 (kV/cm), are noted on the figure; the electric field is horizontal.

Figure 5 shows experimental results and theoretical calculations for several fluid pairs in this class. The continuous lines are 'least squares' fits of the experimental data and the dashed lines correspond to the theoretically predicted behaviour. For each fluid pair, the behaviour of 4–10 different drops was measured. According to the results, D and aE_0^2 are linearly related; the agreement with the theory, although far from perfect in some cases, is much improved over that achieved by Torza *et al.* (1971). In some instances the behaviour of our fluids changed when they stood in contact for some time to equilibrate. Evidently the two fluids were not completely immiscible and some constituents partition between the two phases or accumulate on the interface. The notation 'non-equilibrated' and 'equilibrated' is used to distinguish such situations.

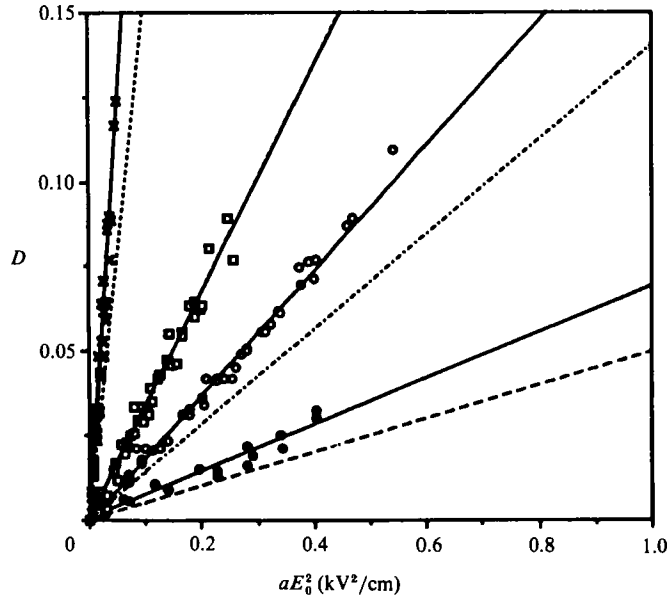

FIGURE 5. Deformation measurements for fluid systems giving prolate deformations: ×, water+Triton drops in castor oil; □, water+Triton drops in silicone oil (125 P) (equilibrated); ○, water drops in castor oil; ●, water drops in silicone oil (300 P). Dashed lines represent the theoretical predictions.

Class (ii): $R \ll 1$. Here the deformation is given by

$$D = \frac{9\epsilon_0 \bar{\epsilon}}{16\gamma} \frac{1}{4} \left\{ S - 2 - 3 \frac{2M+3}{5M+5} \right\} aE_0^2. \tag{14}$$

A fluid system representative of this class is silicone oil (125 P) (the number in parentheses is the nominal viscosity of the fluid) in a mixture of castor oil and the non-ionic surfactant Triton. The host fluid is much more conductive than the drop and deformations are oblate. Results for two systems appear in figure 6. For the silicone oil (125 P) drop in castor oil+Triton the discrepancy between theory and experiment is quite small. The results for the lower-viscosity drop system without surfactant are not in as good agreement with the theory. The reason may be that the conductivity ratio for the silicone oil (10 P)–castor oil system is twice as large and so small changes in the conductivity of the inner fluid alter the size of the deformation substantially. Moreover, as will be discussed shortly, the conductivities of some silicone fluids appear to be field-dependent.

Class (iii): $R = O(1)$. For fluid pairs in this class, accurate measurements of conductivity are necessary since the deformation is sensitive to the magnitude of R. In a typical experiment with silicone oil drops in castor oil, oblate deformations occurred at low field strengths but, as the field increased, the drop became less deformed and eventually turned into a prolate spheroid. The pattern reversed upon lowering the field strength and was reproducible. In this case, changes in deformation might be attributed to the effect of the field on the drop conductivity since separate measurements of the conductivity of the silicone oil disclosed that its conductivity increases by a factor of 2 over this range of field strengths. Independent measurements and *in situ* monitoring of the cell resistance show that the conductivity of the suspending fluid did not change. Thus, as the field strength increases, the

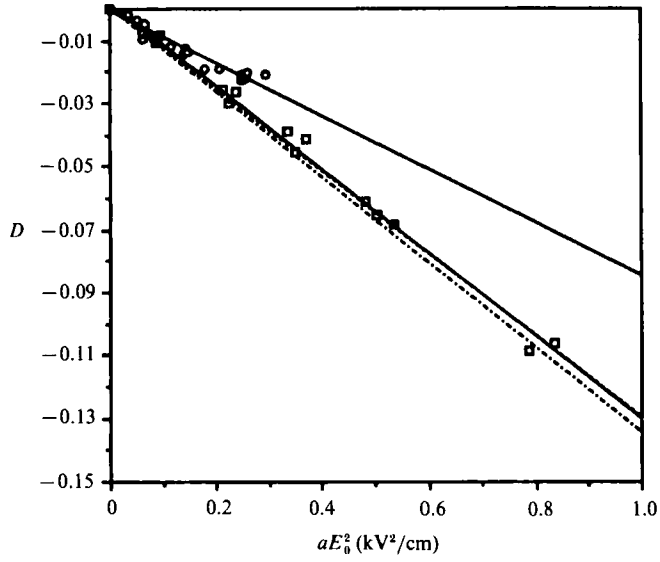

FIGURE 6. Deformation measurements for systems giving oblate deformations: □, silicone oil (125 P) drops in castor oil + Triton; ○, silicone oil (10 P) drops in castor oil. Dashed lines represent the theoretical predictions. The theoretical prediction for the system without surfactant is almost sinvisible since it falls on the line describing the results for the experiments with surfactant.

conductivity ratio would increase from (approximately) 0.5 to 1.0 and, according to the theory, equation (7), the deformation should change from oblate to prolate. We have not yet made an extensive study of deformations for intermediate conductivity ratios due to problems in controlling the conductivity and measuring it accurately.

3.2.1. *Summary of the steady field results*

The results of experiments in steady fields are summarized in table 2. The first data column gives the measured slope, the second lists the calculated slope, the third shows the ratio of these slopes, and the last column gives this ratio for the Torza *et al.* (1971) experiments. Generally, the agreement between theory and experiment is much improved compared to previous work.

3.3. *Drop deformation measurements in oscillatory fields*

In oscillatory fields the electric stresses have time-dependent and time-independent parts so the drop oscillates about a deformed shape. Both time-independent and time-dependent deformations were studied.

3.3.1. *The effect of field strength on the time-independent deformation, D_s*

First we discuss measurements of the time-independent deformation in cases where the frequency is high enough to make the time-dependent deformation negligible. The applied field had a sinusoidal waveform with a frequency of 60 Hz, measured with an oscilloscope through a high-voltage probe connected to the high-voltage electrode and monitored continuously throughout each experiment.

The results of steady deformation measurements are summarized in figure 7, where we see that the leaky dielectric model, modified to take account of the oscillatory field, accurately describes the experimental results. Table 3 summarizes our results and previous experimental work. Here the agreement between theory and experiment is much better than in the steady field experiments. Note also that in the oscillatory

Drop	Outer fluid	Measured slope $m \equiv \frac{D}{aE_0^2}$	Calculated slope $m^* \equiv \frac{9\epsilon_0\epsilon}{16\gamma}\frac{\Phi}{(2+R)^2}$	Ratio m/m^*	Ratio (from Torza *et al.*) m/m^*
Water	Castor oil	0.18	0.135	1.34	2.1
Water	Silicone oil (300 P)	0.062	0.049	1.26	3.8
Water	Silicone oil (1000 P)	0.069	0.049	1.4	3.8
Water + Triton	Castor oil (non equilibrated	2.4	1.5	1.6	2.1†
Water + Triton	Castor oil (equilibrated)	2.07	1.43	1.45	—
Water + Triton	Silicone oil (125 P) (equilibrated)	0.33	0.325	1.02	1.7†
Castor oil	Silicone oil (100 P)	0.32	0.29	1.10	3.8
Silicone oil (50 P)	Castor oil + Triton	−0.125	−0.135	0.93	—
Silicone oil (125 P)	Castor oil + Triton	−0.135	−0.139	0.97	—
Silicone oil (10 P)	Castor oil	−0.084	−0.13	0.65	1.2
Silicone oil (125 P)	Castor oil	−0.089	−0.155	0.57	1.6

† A different surfactant was used for these two cases

TABLE 2. Drop deformation in steady fields

Drop	Outer fluid	Measured slope $m \equiv \frac{D_s}{aE_0^2}$	Calculated slope $m^* \equiv \frac{9\epsilon_0\epsilon}{16\gamma}\Phi_s$	Ratio m/m^*	Ratio (from Torza *et al.*) m/m^*
Water	Castor oil	0.13	0.13	1.0	2.1
Water + Triton	Castor oil (non-equilibrated)	1.78	1.48	1.2	2.1†
Water + Triton	Castor oil (equilibrated)	1.77	1.48	1.2	—
Castor oil	Silicone oil (100 P)	0.011	0.009	1.22	1.5
Silicone oil (125 P)	Castor oil + Triton	−0.122	−0.12	1.02	

† A different surfactant was used

TABLE 3. Drop deformation in oscillatory fields

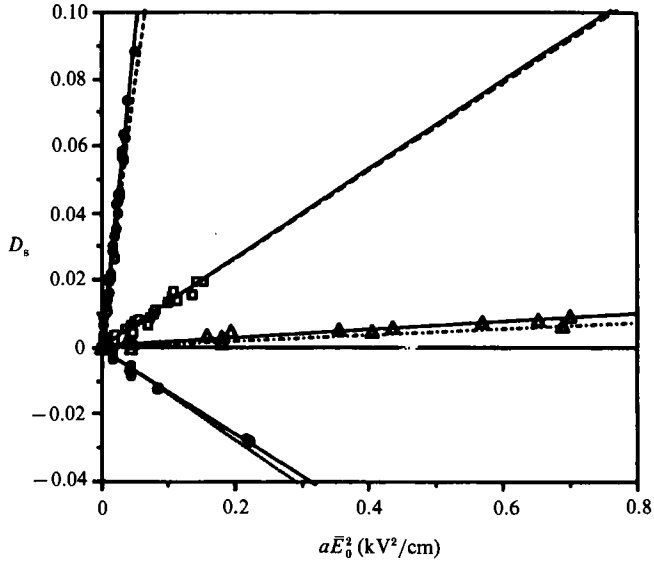

FIGURE 7. Deformation measurements in oscillatory fields: ○, water+Triton drops in castor oil; □, water drops in castor oil: △, castor oil drops in silicone oil (100 P); ●, silicone oil (125 P) drops in castor oil+Triton. Dashed lines represent the theoretical predictions.

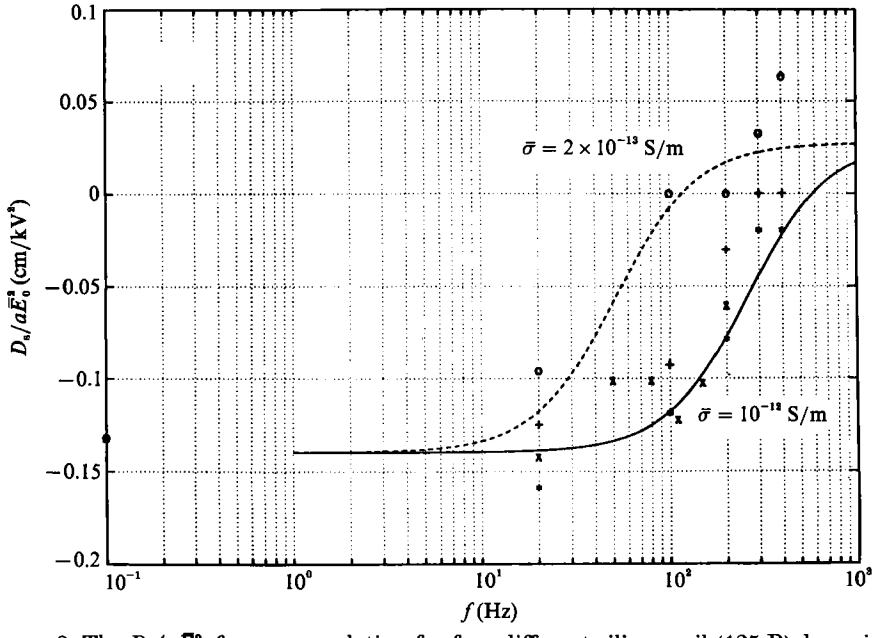

FIGURE 8. The $D_s/a\bar{E}_0^2$–frequency relation for four different silicone oil (125 P) drops in castor oil; the electric field is maintained constant and the frequency increases from 0 to 400 Hz. The curves correspond to the theoretically predicted values for two different values of the drop conductivity, $\bar{\sigma} = 10^{-12}$ S/m and 2×10^{-13} S/m; the different symbols represent different drops. $R = 10^5$.

field experiments, fresh and pre-equilibrated water+Triton–castor oil systems give the same deformation whereas in the steady field experiments significant differences existed. We suspect that this agreement may be due to the absence of significant interfacial composition gradients in the oscillatory experiments.

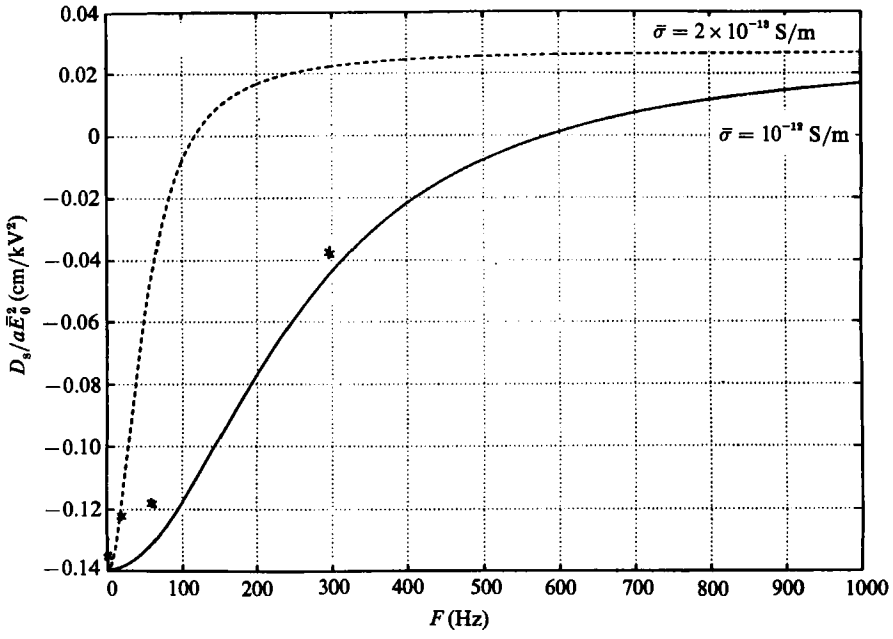

FIGURE 9. The $D_s/a\bar{E}_0^2$–frequency relation for silicone oil (125 P) drops in castor oil. As the electric field was systematically increased the slope of the $D_s/a\bar{E}_0^2$ relation was measured at four different frequencies (asterisks). The curves are the theoretically predicted slopes for two different values of the drop conductivity: $\bar{\sigma} - 10^{-12}$ S/m and 2×10^{-13} S/m. $R = 10^5$.

3.3.2. *The effect of frequency on the time-independent deformation, D_s*

The effect of frequency on the time-independent deformation was studied with the silicone oil (125 P)–castor oil system. Two sorts of experiments were carried out. In the first set, the field intensity was held constant while the frequency increased from 0 to 400 Hz. Increasing the frequency diminishes the extent of the oblate deformation with this system. The results for four different drops appear in figure 8. Observe that the theoretical deformation is very sensitive to the inner fluid conductivity. Some of the scatter may be due to small changes in the conductivity in addition to the fact that the deformations are small.

In the second set of experiments, the frequency was kept constant while the amplitude of the field varied from 0 to 3.35 kV/cm. Measurements were made at frequencies of 0, 20, 60, and 297 Hz; four to six drops were studied at each frequency. The results are summarized on figure 9. The deformation decreases with increasing frequency, in agreement with the predictions of the model, and the overall agreement between theory and experiment is fairly good; deviations from the theory are less than 20%. If the conductivity were to increase with frequency, this would explain why the experimental points are close to the curve corresponding to $\bar{\sigma} = 2 \times 10^{-13}$ S/m at low frequencies and closer to the curve corresponding to $\bar{\sigma} = 10^{-12}$ S/m at higher frequencies.

3.3.3. *The effect of frequency on the time-dependent total deformation, D*

The effect of frequency on the time-dependent deformation was studied for the system castor oil–silicone oil (100 P). This pair of fluids yields prolate deformations in steady fields with calculated deformations in close agreement with the theory (cf.

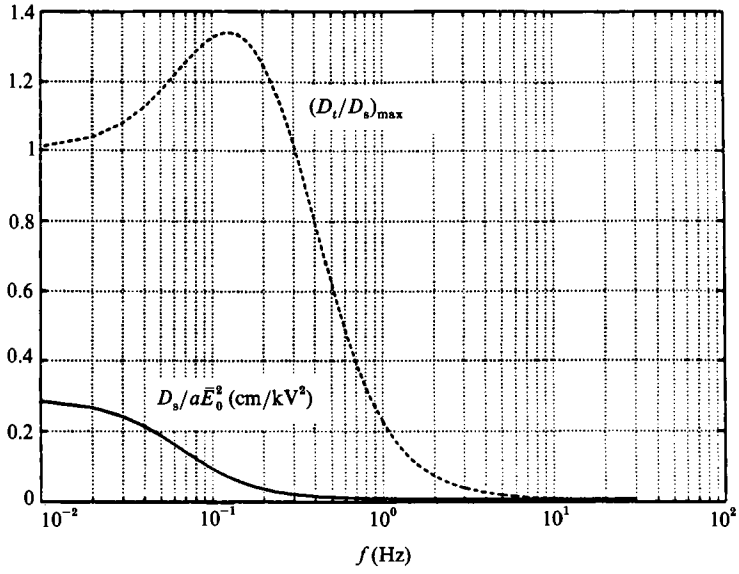

FIGURE 10. The $(D_t/D_s)_{max}$–frequency relation for castor oil drops in silicone oil (100 P).

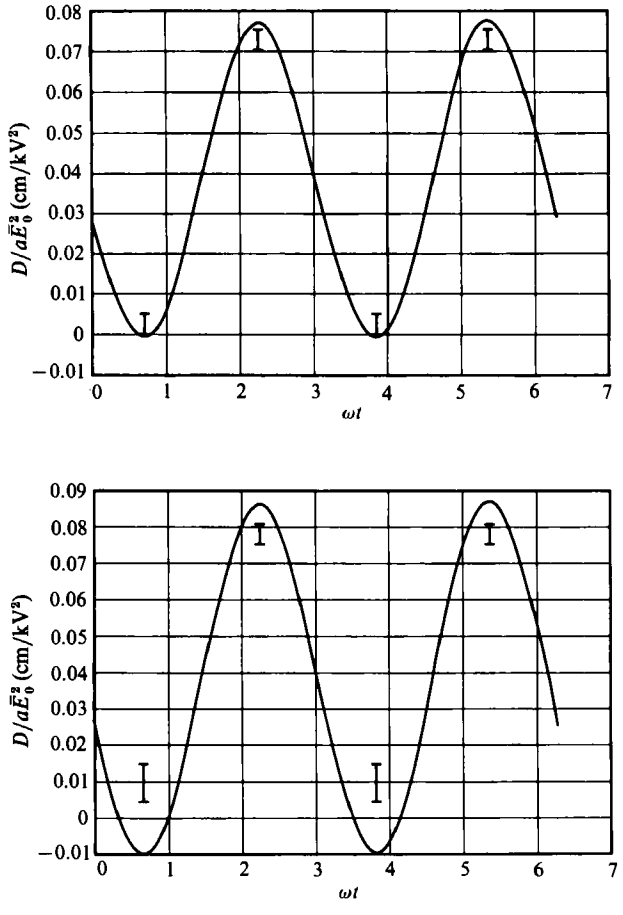

FIGURE 11. Maximum and minimum total deformation, as measured for castor oil drops in silicone oil (100 P). The curves depict the theoretically predicted behaviour.

table 2). To study time-dependent deformations conditions must be selected where the oscillatory part is at least as large as the steady component. Figure 10, which depicts different components of the deformation predicted by the leaky dielectric theory, indicates that the time-dependent deformation is as large as the steady part below 0.3 Hz. The main experimental limitation is that the total deformation is small. After releasing a castor oil drop in the silicone oil, the field amplitude was increased systematically from 0 to 5.9 kV/cm with the frequency set at 0.19 Hz. Drop motion was recorded on video tape at selected field strengths. Then, to provide data on the maximum and minimum deformations corresponding to a given field strength, images were captured at the appropriate times using the Matrox frame grabber; $D/a\bar{E}_0^2$ was calculated from the experimental data at several different field strengths. Figure 11 shows the theoretical $\cos(2\omega t+\beta)$ deformation calculated from equation (12) along with the measured maximum and minimum deformations over one cycle. Data were pooled from several cycles so as to provide error estimates as indicated by the error bars on the figure. Note that the prolate deformation oscillates between the maximum and a minimum where the droplet is nearly spherical. As the figure shows, the experimental data are in good agreement with the theoretical predictions.

4. Discussion

Although agreement between theory and experiment is rather good, some discrepancies remain. Aside from the usual problems, the differences could arise from: (i) inhomogeneity of the electric field, (ii) field-dependent interfacial tension, (iii) surface conductance and charge convection on the interface, (iv) interfacial tension gradients. In our experiments we attempted to avoid electric field inhomogeneities by using small droplets placed near the centre of the cell but items (i) and (ii) surely deserve further study. In some experiments drop migration was observed so special care was taken to ensure that this did not influence deformation (by capturing the image rapidly, before large-scale motion developed). In recent experiments (in our laboratory by S. Sankaran) it was found that in some cases a large-scale bulk motion develops after several minutes of exposure to the field. This motion arises from the action of the field on the free charge at the air–liquid interface at the top of the cell but it can be arrested by using a lid on the cell to stop lateral motion of the interface. Deformations measured over a period of several minutes with a lid in place are the same as those measured in its absence.

Item (iii) *Surface conductance and charge convection.* A finite surface conductivity could change the magnitudes of the charges facing the electrodes and produce changes in the deformation (Torza *et al.* 1971). However, although the deformation would be linear in E_0^2 it would not be linear in aE_0^2. Our results do not show any systematic deviation from linearity when both E_0^2 and a are varied. Nevertheless, since the experiments cover only a small range of drop radii (0.2 to 0.56 mm), field strength effects are dominant. More experiments are needed to elucidate this matter.

Item (iv) *Interfacial tension gradients.* To estimate the effect of interfacial tension gradients we constructed a simple model based on the behaviour of an insoluble surfactant. Of course, Triton, the surfactant used here, is partially soluble, so any interfacial tension gradients in our experiments are further modulated by transport through the bulk. Nevertheless, the simple model serves to show that interfacial tension gradients tend to increase the deformation. According to the model outlined in the Appendix, the deformation in the presence of interfacial tension gradients due

to an insoluble surfactant (one that remains confined to the interface) will be the same as that given by (7), except that the discriminating function is

$$\Phi = S(R^2+1)-2+\frac{2(SR-1)\left[3(2M+3)-\dfrac{\partial\gamma}{\partial C_A}\dfrac{2aC_{A_e}}{\bar{\mu}D_s}\right]}{\left[10(M+1)-\dfrac{\partial\gamma}{\partial C_A}\dfrac{2aC_{A_e}}{\bar{\mu}D_s}\right]}. \tag{15}$$

Here C_{A_e} denotes the interfacial concentration of surfactant with surface diffusivity D_s and $\partial\gamma/\partial C_A$ is the rate of change of interfacial tension with composition.

This expression indicates that interfacial tension gradients ought to produce somewhat larger deformations (recall that $\partial\gamma/\partial C_A$ is usually negative) for prolate or oblate drops. Although knowledge of the surface diffusivity and concentration dependence of the interfacial tension is necessary for a quantitative assessment of the effect, bounds can be estimated by taking the interfacial tension group,

$$2aC_A(\partial\gamma/\partial C_A)/\bar{\mu}D_s,$$

to be zero or infinitely large. The shifts in the deformation calculated in this way are small for the systems studied here. Although deformations slightly larger than theoretical were observed for prolate drops, the oblate deformations were smaller. It seems that interfacial tension gradients play some role in the deformation, but the effect is small for our systems and interfacial tension gradients do not appear to be the source of the discrepancies between theory and experiment observed here.

5. Conclusions

In steady electric fields, the effect of the field magnitude was investigated for a wide range of conductivity ratios; in oscillatory fields the roles of the field magnitude and frequency on the time-dependent and time-independent deformations were studied. The agreement with theoretical predictions is much improved compared to previous studies.

In steady fields: (*a*) the experimentally measured deformations of drops deformed into prolate ellipsoids are 1.02 to 1.6 times the theoretically predicted values; (*b*) for drops deformed into oblate ellipsoids, the experimentally measured deformations are slightly smaller than the theoretically predicted except for situations where the drop conductivity depends on the electric field magnitude.

In oscillatory fields: (*a*) with both prolate and oblate spheroids, the experimentally measured deformations did not deviate from the theoretical predictions by more than 20%; (*b*) the frequency dependence of both time-dependent and time-independent deformations closely follows the 'leaky dielectric model'.

We do not have an explanation as to why previous experimental work showed large discrepancies with the theory. However, the fact that the leaky dielectric model successfully predicts the behaviour for the systems studied here suggests that the next task is to investigate a wider range of fluid properties and refine the experiment to further improve agreement between theory and experiment. An especially important consideration is the control of fluid conductivity.

This work was supported by the NASA PACE program, Contract NAG 2-259. We are also indebted to the Textile Research Institute, Princeton NJ for assistance in measuring the interfacial tensions.

Appendix. Interfacial tension effects

Suppose a surface-active agent is absorbed on the fluid–fluid interface. As fluid elements move along interface, stretching and compression causes changes in surface concentration. Here we consider small changes in surface concentration and ignore any exchange of surfactant molecules with the bulk liquid, i.e. the surfactant resides only at the drop interface. The interfacial tension, γ, depends only on the surface concentration, C_A; all other fluid properties are assumed to be constant. If C_A varies over the interface, so does γ. When surface viscosity is absent, the equations given by Scriven (1960) and Flumerfelt (1980) for equilibrium at the interface are (6) for the normal stress and

$$[T_\theta^{\mathrm{e}}]+[T_\theta^{\mathrm{v}}] = -\frac{1}{r}\frac{\partial\gamma}{\partial\theta}. \tag{A 1}$$

for the tangential component. The distribution of interfacial tension along the drop can be obtained from the dependence of C_{A} on the angle θ, namely

$$C_A = C_{A_{\mathrm{e}}}+C'_A(\theta). \tag{A 2}$$

here $C_{A_{\mathrm{e}}}$ is the concentration of surfactant when uniformly distributed over the interface and C'_A is the local deviation from the uniform value. Moreover,

$$\frac{\partial\gamma}{\partial\theta} = \left(\frac{\partial\gamma}{\partial C_A}\right)\left(\frac{\partial C_A}{\partial\theta}\right), \tag{A 3}$$

where $\partial\gamma/\partial C_A$ is a parameter describing the way the interfacial tension depends on the surfactant concentration; it is usually negative.

The amount of surface-active agent per unit area satisfies the mass conservation law for the surface phase. If the concentration of the surfactant at any point on the interface deviates only slightly from the equilibrium value and there is no net flux of surfactant to or from the bulk solution, then convection and diffusion in the surface are balanced and

$$\boldsymbol{\nabla}_{\mathrm{s}}\cdot(C_A\boldsymbol{u})-\boldsymbol{\nabla}_{\mathrm{s}}\cdot(D_{\mathrm{s}}\boldsymbol{\nabla}_{\mathrm{s}}C_A) = 0. \tag{A 4}$$

D_{s} is the surface diffusion coefficient of the surfactant. Neglecting the product $C'_A\boldsymbol{u}$ yields

$$\frac{1}{r\sin\theta}\frac{\partial}{\partial\theta}[C_{A_{\mathrm{e}}}u_\theta\sin\theta] = \frac{D_{\mathrm{s}}}{r^2}\frac{\partial}{\partial\theta}\frac{\partial}{\partial\theta}\left[\sin\theta\frac{\partial C'_A}{\partial\theta}\right] \tag{A 5}$$

and since

$$u_\theta = 2A\sin\theta\cos\theta \tag{A 6}$$

the surfactant concentration varies over the surface as

$$\frac{\partial C'_A}{\partial\theta} = \frac{2aAC_{A_{\mathrm{e}}}}{D_{\mathrm{s}}}\cos\theta\sin\theta. \tag{A 7}$$

Owing to the motion induced by the electric field, surfactant accumulates at the poles or the equator of the drop depending on the sign of A. Increasing the surfactant concentration leads to a decrease of the interfacial tension and at such points the interface has a higher curvature (larger deformation) to keep the stresses balanced.

If we denote the coordinate of the point where the interfacial tension is equal to the uniform surfactant distribution, $\gamma_{\theta e}$, by θ_e, then the interfacial tension at any other point is given by

$$\gamma(\theta) = \gamma_{\theta_e} - \frac{\partial \gamma}{\partial C_A} \frac{aAC_{A_e}}{D_s} \cos^2\theta \Big|_{\theta_e}^{\theta}. \tag{A 8}$$

From the expression for γ and the tangential stress balance, (A 1), we find

$$A = -\frac{9a\epsilon_0 E_0^2 \bar{\epsilon}}{2(2+R)^2} \frac{2(SR-1)}{\left[10(\mu+\bar{\mu}) - \dfrac{\partial \gamma}{\partial C_A} \dfrac{2aC_{A_e}}{D_s}\right]}. \tag{A 9}$$

Together, (A 6) and (A 9) show that the presence of surfactant causes a retardation of fluid motion, a common effect of contamination in liquid interfaces (Stone & Leal, 1990). The normal stress balance leads to expressions for the deformation except that now the discriminating function is given by (15).

REFERENCES

Adamson, A. W. 1967 *Physical Chemistry of Surfaces*, 2nd edn, Interscience.

Ajayi, O. O. 1978 A note on Taylor's electrodynamic theory. *Proc. R. Soc. Lond.* A **364**, 499–507.

Allan, R. S. & Mason, S. G. 1962 Particle behaviour in shear and electric fields. I. Deformation and burst of fluid drops. *Proc. R. Soc. Lond.* A **267**, 45–61.

American Institute of Physics 1972 *American Institute of Physics Handbook*, vol. 5, pp. 123, 133. McGraw-Hill.

Arp, P. A., Foister, R. T. & Mason, S. G. 1980 Some electrohydrodynamic effects in fluid dispersions. *Adv. Colloid Interface Sci.* **12**, 295–356.

ASTM 1987 *Annual Book ASTM Standards* D 924-82b A-C loss characteristics and relative permittivity (dielectric constant) of electrical insulating liquids. pp. 147–156.

Basaran, O. A. & Scriven, L. E. 1988 The Taylor pump: viscous free surface flow driven by electric shear stress. *Chem. Engng Commun.* **67**, 259–273.

Baygents, J. C. & Saville, D. A. 1989 The circulation produced in a drop by an electric field: A high field strength electrokinetic model. In *Drops & Bubbles: Third Intl Colloq.* (ed. T. Wang), pp. 7–17, American Institute of Physics.

Davies, J. T. & Rideal, E. K. 1963 *Interfacial phenomena*, 2nd edn. Academic.

Flumerfelt, R. W. 1980 Effects of Dynamic Interfacial Properties on Drop Deformation and Orientation in Shear and Extensional Flow Fields. *J. Colloid Interface Sci.* **76**, 330–349.

Garton, C. G. & Krasucki, Z. 1964 Bubbles in insulating liquids: stability in an electric field. *Proc. R. Soc. Lond.* A **280**, 211–226.

Hartshorn, L., Parry, J. V. L. & Essen, L. 1955 The measurement of the dielectric constant of standard liquids. *Proc. Phys. Soc. Lond.* B **68**, 422–446.

Larrendo, L. & St. John Manley, R. 1981 Electrostatic fiber spinning from melts: I. Experimental observations on fiber formation and properties, II. Examination of the flow field in an electrically driven jet, III. Electrostatic deformation of a pendant drop of polymer melt. *J. Polymer Sci. Polymer Phys* **19**, 909–940.

Maryott, A. A. & Smith, E. R. 1951 *Table of Dielectric Constants of Pure Liquids.* National Bureau of Standards Circular 514, US Government Printing Office.

Melcher, J. R. 1976 Electric fields and forces in semi-insulating liquids. *J. Electrostat.* **2**, 121.

Melcher, J. R. 1981 *Continuum Electromechanics.* MIT Press.

Melcher, J. R. & Taylor, G. I. 1969 Electrohydrodynamics: a review of the role of interfacial shear stresses. *Ann. Rev. Fluid Mech.* **1**, 111–146.

Miller, B., Penn, L. S. & Hedvat, S. 1983 Wetting force measurements on fibers. *Colloids Surfaces* **6**, 49–61.

MORIYA, S., ADACHI, K. & KOTAKA, T. 1985 Effect of electric field on the morphology of a poly(ethylene oxide) polystyrene blend. *Polymer Commun.* **26**, 235–237.

MORIYA, S., ADACHI, K. & KOTAKA, T. 1986 Deformation of droplets suspended in viscous media in an electric field: I. Rate of deformation, II. Burst behaviour. *Langmuir* **2**, 155–165.

NISHIWAKI, T., ADACHI, K. & KOTAKA, T. 1988 Deformation of viscous droplets in an electric field: poly(propylene oxide)/poly(dimethylsiloxane) systems. *Langmuir* **4**, 170–175.

OGUZ, H. N. & SADHAL, S. A. 1989 Fluid dynamics and stability analysis of a compound drop in an electric field. *Q.J. Mech. Appl. Maths* **42**, 65–83.

O'KONSKI, C. T. & THACHER, H. C. 1953 The distortion of aerosol droplets by an electric field. *J. Phys. Chem.* **57**, 955–958.

SCRIVEN, L. E. 1960 Dynamics of a fluid interface. *Chem. Engng Sci.* **12**, 98–108.

SCOTT, T. C. & WHAM, R. M. 1989 An electrically driven multistage countercurrent solvent extraction device: the emulsion phase contactor. *Ind. Engng Chem.* **28**, 94.

SHERWOOD, J. D. 1988 Break-up of fluid droplets in electric and magnetic fields. *J. Fluid Mech.* **188**, 133–146.

STONE, H. A. & LEAL, L. G. 1990 The effects of surfactants on drop deformation and breakup. *J. Fluid Mech.* **220**, 161–186.

TAYLOR, G. I. 1966 Studies in electrohydrodynamics. I. The circulation produced in a drop by an electric field. *Proc. R. Soc. Lond.* A**291**, 159–166.

TORZA, S., COX, R. G. & MASON, S. G. 1971 Electrohydrodynamic deformation and burst of liquid drops. *Phil. Trans. R. Soc. Lond.* **269**, 259–319.

VENUGOPAL, G., KRAUSE, S. & WNEK, G. E. 1989 Modification of polymer blend morphology using electric fields. *J. Polymer Sci.* C: *Polymer Lett.* **27**, 497–501.